

Anomalous collective diffusion of interacting run-and-tumble particles

Tanmoy Chakraborty and Punyabrata Pradhan

*Department of Physics of Complex Systems, S. N. Bose National Centre for Basic Sciences,
Block-JD, Sector-III, Salt Lake, Kolkata 700106, India*

We characterize the collective motion of interacting run-and-tumble particles (RTPs) by calculating the bulk-diffusion coefficient in two minimal model systems, for arbitrary density ρ and tumbling rate γ , and offer a generic mechanism to account for the early-time anomalous relaxations in such systems. In the strong-persistence limit of $\gamma \rightarrow 0$, the fascinating interplay between persistence and interaction is quantified in terms of two length scales - “mean free path” and persistence length $l_p = v/\gamma$, with v being the self-propulsion speed. Indeed we show that the bulk-diffusion coefficient has a scaling form $D(\rho, \gamma) = D^{(0)}\mathcal{F}(\rho v/\gamma)$, where $D^{(0)}$ is proportional to the diffusivity of noninteracting particles; the scaling function $\mathcal{F}(\psi)$ is calculated analytically for one model and numerically for the other. In this limit, we find that the bulk-diffusion coefficient varies as a power law in a wide range of density: $D \propto \rho^{-\alpha}$, with exponent α gradually crossing over from $\alpha = 2$ at high densities to $\alpha = 0$ at low densities. As a result, the density relaxation is governed by a nonlinear diffusion equation with anomalous spatiotemporal scaling that can even be ballistic in certain regimes. Our arguments, as demonstrated in simulations, are rather generic, being independent of dimensions and microscopic details.

Introduction.— Transport characteristics of self-propelled particles (SPPs) never cease to surprise [1]; they are often anomalous, indicating the presence of nontrivial correlations and serving as the rule rather than the exception. Anomalous transport in such systems, ranging from living to non-living matter (e.g., bacterial colonies and active Janus particles, respectively), has been investigated in a variety of experiments [2–12], simulations [13–15], and theory [16–19]. For instance, a recent experiment on the expansion of localized Janus swimmers on a two-dimensional substrate was found to exhibit an early-time ballistic growth [20], with the width of the density perturbation growing with time t as $\sim t^{1/z}$, characterized by the dynamic exponent $z = 1$ (ultimately crossing over to normal diffusion with $z = 2$). In a related simulation study of single-file transport of interacting SPPs, the space-time scaling of the two-point density correlations in the early-time regimes was shown to display superdiffusion with $z \approx 1.67$ [21]. Presently it is unclear precisely what causes the anomalous growth, the resultant exponent, and whether or not one should expect a universal behavior. Despite recent progress [22–28], a good theoretical understanding of the time-dependent properties of interacting SPPs, taking into consideration *many-body correlations*, is missing.

In this Letter, starting from a many-particle description of a subclass of SPPs - called run-and-tumble particles (RTPs), we provide a hitherto unexplored hydrodynamic theory that captures the anomalous collective relaxations described above. The studies of dynamical features of SPPs have generally been streamlined into characterizing self diffusion and related quantities [18, 29–39]. However the *bulk-diffusion coefficient* D , governing collective diffusion through Fick’s law for particle current

$$J_D = -D \frac{\partial \rho}{\partial X} \quad (1)$$

due to density gradient $\partial \rho / \partial X$, remains mostly un-

explored. Indeed characterizing bulk diffusion in interacting-particle systems is of fundamental interest in statistical physics and a crucial first step in formulating fluctuating hydrodynamics [40, 41]. However, despite significant progress made in the past [42, 43], exact results for systems - particularly SPPs, that have many-body correlations, are rare and limited only to systems with a product-measure steady state [24, 44, 45] and that with one [46] or two particles [23, 47, 48]. There are phenomenological theories [49, 50], whose validity, however, has not been tested through rigorous calculations and first-principle characterization of collective diffusion in standard models of interacting SPPs remains a long-standing issue. Here, from microscopic dynamical calculations, we characterize collective diffusion in *strongly persistent* interacting RTPs in d dimensions. We show that there exists a scaling function $\mathcal{F}(\psi)$ governing large-scale relaxation through a precise scaling of the bulk-diffusion coefficient,

$$D(\rho, \gamma) = D^{(0)}\mathcal{F}\left(\frac{\rho v}{\gamma}\right), \quad (2)$$

where ρ , v and $\tau_p = \gamma^{-1} \gg 1$ are density, self-propulsion speed, and persistence time (equivalently, persistence length $l_p = v\tau_p$), respectively; moreover, we analytically calculate $\mathcal{F}(\psi)$ for an idealized version of RTPs. These are the main result of the Letter. The scaling variable $\psi = \rho v/\gamma$ quantifies the interplay between persistence and interaction, with the prefactor $D^{(0)} = v^2/\gamma d$ proportional to the diffusivity in noninteracting limit. Although persistent random walks are long known [51, 52], this particular scaling function, to the best of our knowledge, has not yet been reported in the literature.

Our central idea is that collective transport in the strong-persistence limit, with $l_p \gg r_0$ - the particle diameter, is governed by two length scales, “mean free path” and persistence length; as a result, the bulk-diffusion coefficient has a highly nonlinear (power-law)

density dependence, accounting for the previously observed early-time (roughly, at the onset of diffusion) anomalous growth. We also show that the early-time relaxation of initially localized density profiles are *non-Gaussian*, where their spatiotemporal scaling form can be determined within the theory. Our results suggest that the related growth exponent is *not* universal, but rather depends on specific parameter regimes. Our findings, as succinctly expressed in Eq. (2), are of particular significance: They are independent of dimensions and microscopic details and unveil a unique mechanism of collective transport - *diffusive, yet anomalous* - that has not been identified previously in SPPs. Notably, the exact functional form of $\mathcal{F}(\psi)$ depends on microscopic details.

Let us begin by presenting the scaling argument and the mechanism of nonlinear diffusion. The RTPs move ballistically with a characteristic speed v (called “run”) and then randomly change direction (called “tumble”) with rate $\gamma = 1/\tau_p$. Particles also interact with their neighbors, for example, through excluded-volume, or hardcore, interactions, as considered here. We do not, however, consider thermal diffusion, being irrelevant in the strong-persistence regime. For simplicity, consider N such hardcore particles on d -dimensional periodic hypercubic lattice of size L and volume $V = L^d$ where the global number density $\rho_0 = N/V$. The propulsion directions of particles randomly orient towards any of the $2d$ possible directions. We note that there are only two relevant length scales: the persistence length $l_p = v/\gamma$ and the mean gap $\langle g \rangle$ (equivalently, a “mean free path”) between two consecutive particles along a particular direction of motion. Indeed, it makes no difference where the neighboring particles are (as defined by the inter-particle spacing); the physics is determined by how far, on average, the next particle is in the direction of a moving one and remains unchanged when these two length scales are rescaled. Therefore, from dimensional ground, any quantities should be constructed by combining the two length scales l_p and $\langle g \rangle$. This implies that the bulk-diffusion coefficient can be cast in a form $D = D^{(0)}\mathcal{F}(l_p/\langle g \rangle)$, where scaling function $\mathcal{F}(\psi)$ depends on a *single* dimensionless scaling variable $\psi = l_p/\langle g \rangle = v/\langle g \rangle\gamma$ with the prefactor $D^{(0)} = \gamma l_p^2 = v^2/\gamma$. Furthermore, in the low-density limit, as the average number of particles in any row (consisting of L sites) is equal to $L/\langle g \rangle$ and therefore $(L/\langle g \rangle) \times (L^{d-1}/a) = N$, we obtain an exact relation,

$$\langle g \rangle = \frac{1}{\rho_0 a}, \quad (3)$$

where $a \sim r_0^{d-1}$ and r_0 are particle cross-section and diameter, respectively; we put $a = 1$ on a hypercubic lattice of unit spacing. The above relation immediately leads to Eq. (2). The asymptotic form of $\mathcal{F}(\psi)$ is determined as follows. In *noninteracting* limit $\rho_0 \ll 1$ and $\langle g \rangle \gg l_p$, we have $D \sim l_p^2/\tau_p \sim 1/\gamma$, implying $\mathcal{F}(\psi) = \text{const.}$ as $\psi \rightarrow 0$. However, in *strongly interacting* limit $l_p \gg \langle g \rangle$, D is proportional to γ as microscopic events occur on a

time scale $\tau_p = \gamma^{-1}$, implying $\mathcal{F}(\psi) \sim 1/\psi^2$ as $\psi \rightarrow \infty$. This explains the power-law dependence of D on ρ and, as we demonstrate later, the anomalous early-time relaxations. The above arguments, although plausible, must be validated, which we do next.

Hydrodynamics.— Hydrodynamics deals with large-scale spatiotemporal properties of slow variable(s). As particle number is conserved, on a time scale much larger than the persistence time, particle density $\rho(X, t)$ is the only slow variable in the system. In that case, density relaxation is governed by diffusive processes and, using Eq. (1) and continuity equation, we can write the time-evolution of local density,

$$\frac{\partial \rho(X, t)}{\partial t} = \nabla \cdot [D(\rho, \gamma) \nabla \rho], \quad (4)$$

which, due to an explicit density dependence of the bulk-diffusion coefficient, is governed by a nonlinear diffusion equation and has interesting consequences. We verify the hydrodynamic description for two minimal models of interacting RTPs both in one (1D) and two (2D) dimensions, having the *necessary ingredients* - (i) a typical persistence length and (ii) excluded-volume interaction.

Long-ranged lattice gas.— We consider a long-ranged lattice gas (LLG) of N hardcore particles on a d -dimensional periodic hypercubic lattice of length L . With unit rate, a particle attempts to hop, symmetrically along any one of the $2d$ directions, by hop-length l drawn from an exponential distribution $\phi(l) \propto \exp(-l/l_p)$. Provided that the stretch of consecutive vacancies from the particle along the hopping direction, called the *gap*, is at least of length l (i.e., if gap size $g \geq l$), the attempted hop is successful; otherwise, due to the hard-core constraints, the particle traverses the entire stretch and sits adjacent to its nearest occupied site. Clearly, the long-ranged hopping mimics the ballistic “run” of micro-swimmers, having random (exponentially distributed) “run”-lengths with a typical persistence length l_p , and is expected to capture collective behavior of RTPs on the persistence time-scale τ_p . Despite its simplicity, the LLG does not have a product-measure steady-state and generates non-trivial spatial correlations, resulting in clustering and large density fluctuations.

Bulk-diffusion coefficient.— An advantage in dealing with LLG is that the system possesses a *gradient property* [44], allowing for local instantaneous current to be expressed as the gradient of a local observable and for the bulk-diffusion coefficient to be exactly determined in terms of the steady-state gap distribution $P(g)$. We provide below the results and a sketch of the calculations; see appendix Sec. A for details. When a particle makes a long-ranged hop to reach its destination, it jumps over all vacant sites in between; thus, current across all such bonds increases (decreases) by unity for a rightward (leftward) hop. Defining net cumulative current $\langle Q_X(t) \rangle$ across a bond $(X, X+1)$ up to time t , we obtain instantaneous current $J_D = d\langle Q_X(t) \rangle/dt = \frac{1}{2d} \sum_{l=1}^{\infty} \phi(l) \left[\sum_{g=1}^{l-1} \left(\mathcal{V}_{X+g+1}^{(g+2)} - \mathcal{V}_{X+1}^{(g+2)} \right) + \left(\mathcal{U}_{X+l}^{(l)} - \mathcal{U}_X^{(l)} \right) \right],$

where $\mathcal{U}^{(l)}$ and $\mathcal{V}^{(l+2)}$ are the probabilities of having l consecutive sites vacant and of having a hole cluster of size l , respectively. By performing gradient expansions and some algebraic manipulations, the current is shown to obey Eq. (1) with the bulk-diffusion coefficient in d dimensions given by

$$D_{LLG}(\rho, \gamma) = -\frac{1}{2d} \frac{\partial(\rho u)}{\partial \rho}, \quad (5)$$

where $u(\rho, \gamma) = \sum_{l=1}^{\infty} \phi(l) [\sum_{g=1}^{l-1} gP(g) + l \sum_{g=l-1}^{\infty} (g-l+1)P(g)]$ depends on both density and persistence length. Of course, explicit calculation of $P(g)$ is difficult in general. However, $P(g)$ for large g is expected to be an exponential $P(g) \simeq N_* e^{-g/g_*}$, where $N_*(\rho, \gamma)$ and $g_*(\rho, \gamma)$ are the proportionality constant and typical gap size, respectively; N_* is determined from the normalization condition $\sum_g P(g) = 1$ and Eq. (3). Now following the previously mentioned scaling argument, also the typical gap size should have a scaling form, $g_* \simeq \rho^{-1} \mathcal{G}(\psi)$, with $\psi = \rho v / \gamma = l_p \rho$; these assertions are verified in simulations, see appendix Sec. B for details. The prefactor $1/\rho$ is fixed from the fact that in the limit $\psi \rightarrow 0$, the system reduces to a noninteracting one and therefore $\mathcal{G}(0) = 1$ [54]. Moreover, in this limit, we see that $u = (1/\rho - 1)$ and, from Eq. (5), $D = \text{const.}$ - a known result for symmetric simple exclusion process. Furthermore, we show that there exists a scaling limit of $\gamma \rightarrow 0$ and $\rho \rightarrow 0$ with $\psi = \rho v / \gamma$ fixed, for which the scaled bulk-diffusion coefficient $D_{LLG}(\rho, \gamma) / D_{LLG}^{(0)} \equiv \mathcal{F}_{LLG}(\psi)$ is a function of a single scaling variable ψ where

$$\mathcal{F}_{LLG}(\psi) = \frac{\mathcal{G}^2(\psi)}{(\mathcal{G}(\psi) + \psi)^3} \left(1 - \psi \frac{\mathcal{G}'(\psi)}{\mathcal{G}(\psi)} \right) \quad (6)$$

and $D_{LLG}^{(0)} = l_p^2 / d$, see appendix Sec. C for details.

For the purpose of illustration, we consider below the LLG in 1D. In the limit of ψ large, as shown in [55], the typical gap size in 1D is given by $g_* = \sqrt{\psi} / \rho$. Thus, combining the two limiting behaviors for small and large ψ , we have $\mathcal{G}(\psi) \simeq (1 + \psi)^{1/2}$, which is then substituted in Eq. (6) to explicitly obtain the scaling function,

$$\mathcal{F}_{LLG}(\psi) = \frac{(2 + \psi)}{2(\psi + \sqrt{1 + \psi})^3}. \quad (7)$$

Note that, for $\psi \ll 1$, $\mathcal{F}_{LLG}(\psi) = 1$ and consequently $D_{LLG} \simeq l_p^2$, which diverges when the persistence length $l_p \rightarrow \infty$; for $\psi \gg 1$, $\mathcal{F}_{LLG}(\psi) \simeq 1/2\psi^2$ and $D_{LLG} \simeq 1/2\rho^2$. In Fig. 1, we plot $D_{LLG}(\rho, \gamma) / D_{LLG}^{(0)}$ as a function of $\psi = \rho v / \gamma$, by numerically calculating D_{LLG} from Eq. (5) through $P(g)$ obtained from simulations (points) for both 1D and 2D. Indeed we observe a nice scaling collapse and see an excellent agreement with $\mathcal{F}_{LLG}(\psi)$ as in Eq. (7), plotted in top-left panel (black solid line).

Model of RTPs. - Next we study the paradigmatic model of hardcore RTPs, each of which is associated with a spin variable, on a d -dimensional periodic lattice

of length L [56]. A particle hops to its nearest neighbor, provided the destination site is vacant, with unit rate along its spin direction (run) and, with rate γ , its spin flips (tumble); in this time unit, $v = 1$. According to our scaling argument, in this case too, the scaled bulk-diffusivity $D_{RTP} / D_{RTP}^{(0)} = \mathcal{F}_{RTP}(\rho v / \gamma)$ should be expressed in terms of a scaling function, which we check next. As an analytic calculation of D_{RTP} for arbitrary densities and tumbling rates is not possible at this stage, we resort to an efficient simulation technique described below [57].

Bulk-diffusion coefficient of RTPs. - To this end, we study the relaxation of a long wave-length (sinusoidal) initial density perturbation $\delta\rho(x, 0) = \rho(x, 0) - \rho_0 \equiv A(0) \sin(2\pi x)$, with wave number $2\pi/L$, lattice position $X = xL$ and ρ_0 the global density, around which the perturbation is applied. For $d = 2$, perturbation is applied in one spatial direction, while density profile is uniform in the other direction. In the limit of weak perturbation $A(0) \ll \rho_0$, the density profile at sufficiently large time $t = \tau L^2$ can be written as $\delta\rho(x, \tau) = A(\tau) \sin(2\pi x)$, with $A(\tau) = A(0) e^{-\Gamma\tau}$ and the relaxation rate $\Gamma(\rho_0, \gamma) = 4\pi^2 D_{RTP}(\rho_0, \gamma)$. To ensure diffusive relaxation, one should first take the thermodynamic limit ($L, N \rightarrow \infty$ with $\rho_0 = N/L$ fixed) and then vary the tumbling rate γ and analyze the case of $\gamma \ll 1$.

We observe that persistence and hard-core interaction compete with each other: While the former enhances diffusion, the latter diminishes it, resulting in nonmonotonic variation of the bulk-diffusivity as a function of tumbling rate, see appendix Sec. D. Notably, a similar feature is observed in the LLG model upon tuning the persistence length. However, as in the LLG, one can quantify the fascinating interplay between persistence and interaction through the scaling variable $\psi = \rho v / \gamma$ for the RTPs too. In Fig. 1, we plot $D_{RTP}(\rho, \gamma) / D_{RTP}^{(0)} \equiv \mathcal{F}_{RTP}(\psi)$ as a function of $\psi = \rho v / \gamma$ with $D_{RTP}^{(0)} = v^2 / \gamma d$ and observe an excellent scaling collapse both in 1D and 2D. The difference in the microscopic time unit in RTPs and LLG is reflected through the ratio $D_{RTP}^{(0)} / D_{LLG}^{(0)} = \gamma$. Moreover, as in the LLG model, we find that $\mathcal{F}_{RTP}(0) = \text{const.}$ and $\mathcal{F}_{RTP}(\psi) \simeq 1/\psi^2$ for $\psi \gg 1$. This reflects the fact that the LLG and RTP models have remarkably similar features, which is evident upon time rescaling for RTPs: $\gamma t \rightarrow t$, with time measured in the unit of persistence time $\tau_p = \gamma^{-1}$ (see Figs. 1 and 2).

However, strictly in the limit $\gamma \rightarrow 0$, the hydrodynamics for RTPs are not well defined unless time and density are appropriately scaled; this is because the (unscaled) bulk-diffusion coefficient $D(\rho, \gamma) \sim 1/\gamma$ diverges as $\rho \rightarrow 0$ and $D(\rho, \gamma) \rightarrow 0$ for any finite ρ . We therefore scale density and time, $\psi(x, \tilde{\tau}) = \rho(x, \tau) / \gamma$ and $\tilde{\tau} = \tau / \gamma$, respectively, in order to have a well-defined hydrodynamics,

$$\frac{\partial \psi(x, \tilde{\tau})}{\partial \tilde{\tau}} = \frac{\partial}{\partial x} \left[\mathcal{F}_{RTP}(\psi) \frac{\partial \psi(x, \tilde{\tau})}{\partial x} \right]. \quad (8)$$

Similarly, hydrodynamics of the LLG in the limit $l_p \rightarrow$

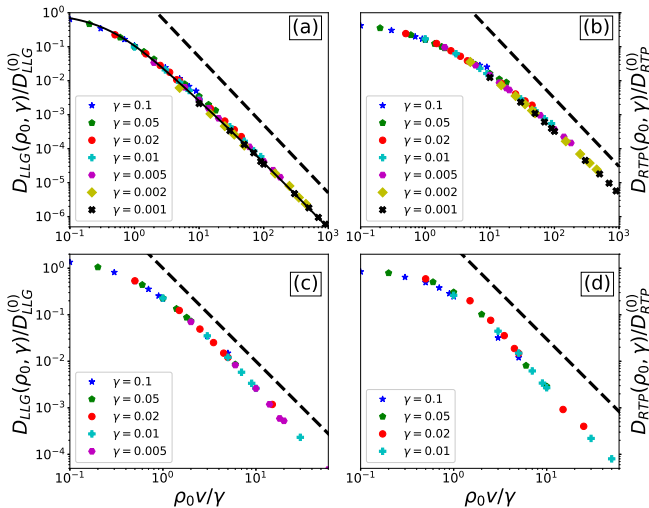


FIG. 1. *Bulk-diffusion coefficient.* We plot scaled bulk-diffusion coefficients $D(\rho_0, \gamma)/D^{(0)}$ as a function of the scaled variable $\psi = \rho_0 v/\gamma$ (with $v = 1$) for the LLG ((a) - 1D and (c) - 2D) and RTPs ((b) - 1D and (d) - 2D). The solid line in panel (a) represents the theory as in Eq. (7); the black dotted guiding lines represent $1/\psi^2$ behavior at large ψ .

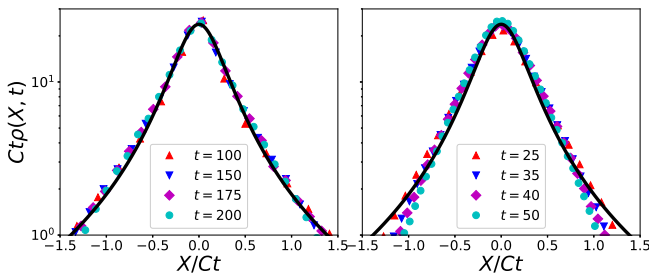


FIG. 2. *Anomalous transport.* We plot scaled density profile $Ctn(X, t)$ against scaled variable $\xi = X/Ct$ for the LLG (left panel) and RTPs (right panel). The spin-flipping rate $\gamma = 0.05$ ($l_p = 20$), $N = 20$ with $C = 2.2$ (for LLG) and 3.2 (for RTPs); the black solid lines - the scaling solution $\mathcal{R}(\xi)$.

∞ is obtained by rescaling $\tilde{\tau} = \tau/\gamma^2$ and replacing $\mathcal{F}_{RTP}(\psi) \rightarrow \mathcal{F}_{LLG}(\psi)$, see appendix Sec. G for details.

Anomalous transport.— Finally, we analyze the issue of the anomalous time evolution of initially localized density profiles in these two models. We first rescale time for RTPs $\gamma t \rightarrow t$ (thus $D \rightarrow \gamma D$), putting the system on an equal footing with the LLG. Now, at the onset of diffusion, i.e., at *early but long enough* time $1 \ll t \ll L^2/D$, particles have undergone many collisions and then local-density can safely be assumed to evolve through Eq. (4). Importantly, depending on density and persistence length, the bulk-diffusion coefficient can have a power-law dependence on density, i.e., $D(\rho) \simeq C/\rho^\alpha$, where the constant C and α ($0 \leq \alpha < 2$) depend on the parameter regime under consideration. Remarkably, Eq. (4) for *delta* initial condition $\rho(X, 0) = \rho_1 \delta(X)$ can be exactly solved through a scal-

ing ansatz $\rho(X, t) = (Ct)^{-\omega} \mathcal{R}(\xi)$, immediately leading to an equation $\omega [\xi \mathcal{R}(\xi)]' = -[\mathcal{R}^{-\alpha} \mathcal{R}'(\xi)]'$ for $R(\xi)$ in terms of a *single* variable $\xi = X/(Ct)^\omega$, where growth exponent $\omega = 1/(2 - \alpha)$ and “prime” denotes derivative wrt ξ ; see Sec. I. For the purpose of demonstration, we choose a regime where $\alpha = 1$ and consequently $\omega = 1$ (thus the dynamic exponent $z = 1/\omega = 1$), implying a ballistic transport, quite strikingly within a framework of a diffusion equation (4), albeit a nonlinear one. By using conditions $\mathcal{R}(0) = 2/\xi_0^2$ and $\mathcal{R}'(0) = 0$, we exactly obtain with constant ξ_0 fixed through conservation condition $\int_{-\infty}^{\infty} \mathcal{R}(\xi) d\xi = \text{const.}$; in particular, for $\xi \gg 1$, $R(\xi) \sim 1/\xi^2$ signifies a power-law decay. Thus the density relaxation has anomalous spatiotemporal scaling with a non-Gaussian spread, which however eventually becomes Gaussian (thus normal diffusion with $z = 2$). In Fig. 2, we plot the scaled density profile $Ct\rho(X, t)$, obtained from simulation, as a function of X/Ct in the early-time regime; we have a nice scaling collapse and a reasonable agreement with theory; deviations at the tails are because the power-law behavior of $D(\rho)$ is cut off at very low densities.

Summary.— We study paradigmatic models of interacting RTPs and characterize collective diffusion, which is caused by subtle many-body effects arising from an intriguing interplay between interaction and persistence. The many-body correlations manifest themselves through anomalous transport and emerge through the competition between two length scales - the “mean free path” and the persistence length, resulting in a hitherto undiscovered scaling of the bulk-diffusion coefficient as encapsulated in the scaling function in Eq. 2. Indeed, local structural relaxations are sensitive to local densities and produce a wide range of time scales (power-law distributed), thus resulting in dynamical heterogeneity and anomalous transport. Notably, the order of hydrodynamic limits is important. When the large persistence-time limit is taken first, followed by the large system-size limit, the system undergoes a previously studied “jamming” or dynamical arrest [58]. On the other hand, studies in Refs. [24, 28] considered system-size dependent tumbling rate, which, though, differs from the standard versions of SPPs - the main motivation behind our work [30, 49, 50, 56, 59, 60]. In our study, the large system-size limit is taken first, followed by the large persistence-time limit. Indeed, attempts to develop a rigorous hydrodynamic description of SPPs that correspond to this specific order of limit have not been successful so far. Recently, the bulk-diffusion coefficient for a dual version of hardcore RTPs in the leading order of tumbling rate has been calculated [61] and it agrees well with Eq. (2) as $\psi \rightarrow \infty$. However, none of these previous works realized the existence of a generic scaling regime for bulk diffusion, which we identify here. Interestingly, in a different context, a similar scaling regime for the self-diffusion coefficient in variants of SPPs has recently been observed in Ref.[35], which nicely complements our findings. However, the precise relationship between the bulk- and self-diffusion

coefficients currently remains unclear. In this scenario, our proposed mechanism of density relaxations could provide useful insights into collective transport in SPPs and will open up new research avenues.

ACKNOWLEDGMENTS

We thank Subhadip Chakraborti, Arghya Das, Rahul Dandekar and R. Rajesh for discussions. P.P.

gratefully acknowledges the Science and Engineering Research Board (SERB), India, under Grant No. MTR/2019/000386, for financial support. T.C. acknowledges a research fellowship [Grant No. 09/575 (0124)/2019-EMRI] from the Council of Scientific and Industrial Research (CSIR), India.

APPENDIX

In the appendix section, we provide additional calculation and derivation details as well as simulations technique we used for our analysis and results presented in the main text.

A. Derivation of the bulk-diffusion coefficient for LLG for arbitrary density and persistence length

In this section, we provide details of the derivation of the bulk-diffusion coefficient of long-ranged lattice gas (LLG). We first calculate the rate of change of the average time-integrated bond-current $\langle Q_X(t) \rangle$ across the specific bond $(X, X+1)$ and use Eq. (1) in the main text to determine the bulk-diffusion coefficient $D_{LLG}(\rho, \gamma)$ for the LLG model in arbitrary d dimensions. It is worth noting that whenever a particle makes a long-range hop to reach its destination along x direction, it overtakes all the vacant sites in the middle of its journey, and for a rightward (leftward) hop, current across all such bonds increases (decreases) by unity. To that end, we introduce the operators,

$$\hat{U}_{X+l}^{(l)} = \bar{\eta}_{X+1} \bar{\eta}_{X+2} \cdots \bar{\eta}_{X+l}, \quad (9)$$

$$\hat{V}_{X+l+1}^{(l+2)} = \eta_X \bar{\eta}_{X+1} \bar{\eta}_{X+2} \cdots \bar{\eta}_{X+l} \eta_{X+l+1}, \quad (10)$$

where $\mathcal{U}^{(l)} = \langle \hat{U}^{(l)} \rangle$ is the probability that consecutive l sites are vacant and $\mathcal{V}^{(l+2)} = \langle \hat{V}^{(l+2)} \rangle$ is the probability of having a hole cluster of size l . If $Q_l(X, t)$ is the time-integrated current across the bond $(X, X+1)$ up to time t corresponding to the hop-length l , then the total time-integrated current across the same bond, considering all possible hop-lengths, is defined as $Q(X, t) = \sum_{l=1}^{\infty} Q_l(X, t) \phi(l)$. It is to be noted that $Q_X^{(l)}(t)$ increases due to rightward hopping events and for a fixed hop-length l and gap size g , we calculate the net probability of increment for the following two cases,

Case I, $l > g$: In this case, a particle crosses the entire cluster of holes of size g in an infinitesimal time dt , and the current across the g bonds within the cluster is increased by unity. Therefore, the bond $(X, X+1)$ must be within the hole cluster for the increase in $Q_X^{(l)}(t)$ caused by the above move. However, we can keep a specific bond $(X, X+1)$ inside a hole cluster of size g by translating the entire cluster in g different ways, each of which corresponds to a unit increment of $Q_X^{(l)}(t)$. The corresponding probability contribution is given by $\mathcal{P}_{g,R}^> dt$ where,

$$\begin{aligned} \mathcal{P}_{g,R}^> &= \frac{1}{2d} \sum_{k=1}^g \langle \eta_{X+k-g} \bar{\eta}_{X+k-g+1} \bar{\eta}_{X+k-g+2} \cdots \bar{\eta}_{X+k} \eta_{X+k+1} \rangle \\ &= \frac{1}{2d} \sum_{k=1}^g \mathcal{V}_{X+k+1}^{(g+2)}. \end{aligned} \quad (11)$$

Case II, $l \leq g$ - In this case, the particle moves along the right by l distance in time dt , increasing current across the l consecutive bonds along the hopping direction by unity and, consequently, increasing $Q_X^{(l)}(t)$ by unity if the bond $(X, X+1)$ is a part of it. Alternatively, one can fix the bond $(X, X+1)$ and translate the empty lane of size l with the hopping particle located at the leftmost site in l different ways, and for each translation, current $Q_X^{(l)}(t)$ increases by unity, and the corresponding probability is $\mathcal{P}_{g,R}^{\leq} dt$, which we calculate

$$\begin{aligned}
\mathcal{P}_{g,R}^{\leq} &= \frac{1}{2d} \sum_{k=1}^l \langle \eta_{X+k-l} \bar{\eta}_{X+k-l+1} \bar{\eta}_{X+k-l+2} \cdots \bar{\eta}_{X+k} \rangle \\
&= \frac{1}{2d} \sum_{k=1}^l \left(\mathcal{U}_{X+k}^{(l)} - \mathcal{U}_{X+k}^{(l+1)} \right).
\end{aligned} \tag{12}$$

Therefore, the total probability that corresponds to the increment of $Q_X^{(l)}(t)$, considering both the cases and all possible gap sizes, can be written as,

$$\begin{aligned}
\mathcal{P}_R &= \sum_{g=1}^{\infty} \left[\mathcal{P}_{g,R}^> \Theta(l-g) + \mathcal{P}_{g,R}^{\leq} (1 - \Theta(l-g)) \right] \\
&= \frac{1}{2d} \left[\sum_{g=1}^{l-1} \sum_{k=1}^g \mathcal{V}_{X+k+1}^{(g+2)} + \sum_{k=1}^l \left(\mathcal{U}_{X+k}^{(l)} - \mathcal{U}_{X+k}^{(l+1)} \right) \right].
\end{aligned} \tag{13}$$

Similarly, following the same method, the total probability corresponding to the unit decrement of $Q_X^{(l)}(t)$, in an infinitesimal time dt , due to leftward movement of the particle can be calculated to be,

$$\mathcal{P}_L = \frac{1}{2d} \left[\sum_{g=1}^{l-1} \sum_{k=1}^g \mathcal{V}_{X+k+1}^{(g+2)} + \sum_{k=1}^l \left(\mathcal{U}_{X+k}^{(l)} - \mathcal{U}_{X+k}^{(l+1)} \right) \right]. \tag{14}$$

Then the continuous-time evolution for the integrated current $Q_X^{(l)}(t)$, in an infinitesimal time interval dt , provided the hop-length is chosen to be l , can be written as follows:

$$\langle Q_X^{(l)}(t+dt) \rangle = \begin{cases} \langle Q_X^{(l)}(t) \rangle + 1, & \text{prob. } \mathcal{P}_R dt, \\ \langle Q_X^{(l)}(t) \rangle - 1, & \text{prob. } \mathcal{P}_L dt, \\ \langle Q_X^{(l)}(t) \rangle, & \text{prob. } 1 - \Sigma dt, \end{cases} \tag{15}$$

where the sum of probabilities for all possible ways the bond $(X, X+1)$ changes current in the infinitesimal time interval dt is given by,

$$\Sigma = \frac{1}{2d} \left[\sum_{g=1}^{l-1} \sum_{k=1}^g \left(\mathcal{V}_{X+k+1}^{(g+2)} + \mathcal{V}_{X+k}^{(g+2)} \right) + \sum_{k=1}^l \left\{ \left(\mathcal{U}_{X+l-k}^{(l)} - \mathcal{U}_{X+l-k+1}^{(l+1)} \right) + \left(\mathcal{U}_{X+l-k}^{(l)} - \mathcal{U}_{X+l-k+1}^{(l+1)} \right) \right\} \right]. \tag{16}$$

Taking into account all possible hop-length l ranging from 1 to ∞ , the time evolution of the average integrated current $\langle Q_X(t) \rangle = \sum_{l=1}^{\infty} \phi(l) \langle Q_X^{(l)}(t) \rangle$ across $(X, X+1)$ can be written as,

$$\frac{d\langle Q_X(t) \rangle}{dt} = \frac{1}{2d} \sum_{l=1}^{\infty} \phi(l) \left[\sum_{g=1}^{l-1} \left(\mathcal{V}_{X+g+1}^{(g+2)} - \mathcal{V}_{X+1}^{(g+2)} \right) + \left(\mathcal{U}_{X+l}^{(l)} - \mathcal{U}_X^{(l)} \right) \right]. \tag{17}$$

It should be noted that the preceding equation is expressed in terms of the gradient of the observables. We assume the observables are slowly varying in the large time limit, and the spatial variation of $\mathcal{V}_X^{(g+2)}$ and $\mathcal{U}_X^{(l)}$ is governed by the evolution of local density $\rho(X, t)$. To that end, we can write $\mathcal{V}_X^{(g+2)} \equiv \mathcal{V}^{(g+2)}(\rho)$ and $\mathcal{U}_X^{(l)} \equiv \mathcal{U}^{(l)}(\rho)$, and the gradient of local observables can thus be expressed as the gradient of local density ρ ,

$$\frac{d\langle Q_X(t) \rangle}{dt} = J_D(X, t) = \frac{1}{2d} \sum_{l=1}^{\infty} \phi(l) \left[\sum_{g=1}^{l-1} g \frac{\partial \mathcal{V}^{(g+2)}(\rho)}{\partial \rho} + l \frac{\partial \mathcal{U}^{(l)}(\rho)}{\partial \rho} \right] \frac{\partial \rho}{\partial X}. \tag{18}$$

Comparing the above equation with Eq. (1) in the main text and identifying the correlators as a function of gap distribution function $P(g|\rho)$ as,

$$\mathcal{V}^{(g+2)}(\rho) = \rho P(g|\rho), \tag{19}$$

$$\mathcal{U}^{(l)}(\rho) = \rho \sum_{g=l-1}^{\infty} (g-l+1) P(g|\rho), \tag{20}$$

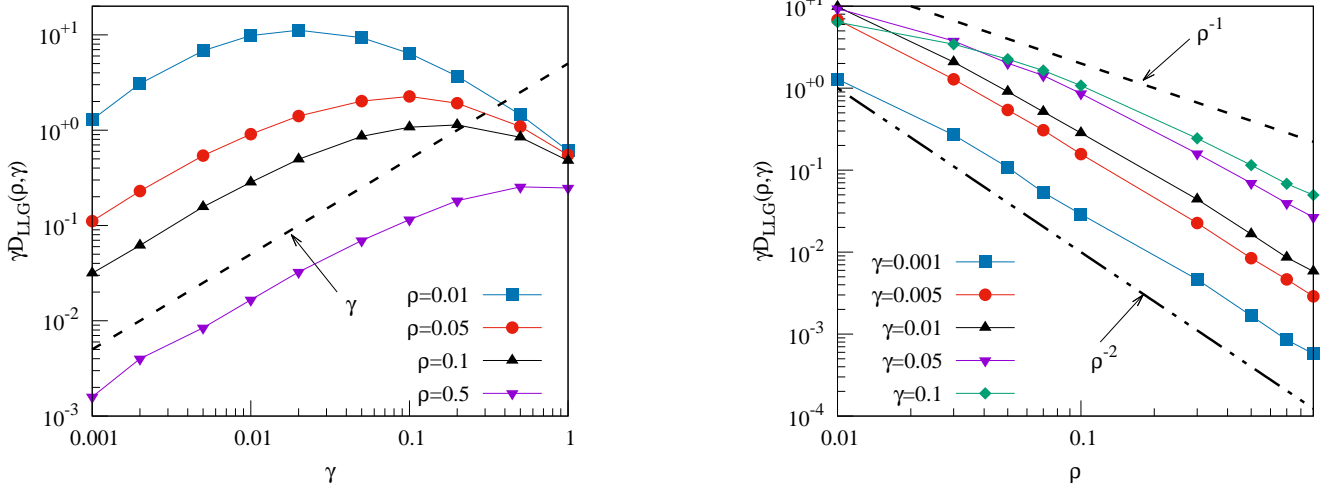


FIG. 3. *Bulk-diffusion coefficient for the LLG model.* In the left-panel, we plot the scaled diffusion coefficient $\gamma D_{LLG}(\rho, \gamma)$ as a function of the inverse persistence hop-length γ for various density $\rho = 0.01$ (blue square), 0.05 (red circle), 0.1 (black up-triangle), 0.5 (magenta down-triangle), while in the right-panel, $\gamma D_{LLG}(\rho, \gamma)$ is plotted against density ρ for different inverse typical hop-length $\gamma = 0.001$ (blue square), 0.005 (red circle), 0.01 (black up-triangle), 0.05 (magenta down-triangle) and 0.1 (green tilted square).

the bulk-diffusion coefficient for the LLG model can be written as,

$$D_{LLG}(\rho, \gamma) = -\frac{1}{2d} \frac{\partial}{\partial \rho} \left[\rho \sum_{l=1}^{\infty} \phi(l) \left(\sum_{g=1}^{l-1} g P(g|\rho) + l \sum_{g=l-1}^{\infty} (g-l+1) P(g|\rho) \right) \right]. \quad (21)$$

This result is shown in the main text in Eq. (5).

In order to calculate $D_{LLG}(\rho, \gamma)$ in arbitrary dimensions using Eq. (21), one first needs to calculate the steady-state gap distribution $P(g)$. For this purpose, we resort to Monte Carlo simulation to calculate $P(g)$ by sampling the vacancy clusters along one of the rectilinear axes (direction of motion of the particles on a hypercubic lattice). Using this method, we calculate the bulk-diffusion coefficient $D_{LLG}(\rho, \gamma)$ in $1D$ and $2D$. In Fig. 3, we show the functional variation of $D_{LLG}(\rho, \gamma)$ in $1D$ in the parameter range $0.01 \leq \rho \leq 0.9$, $0.001 \leq \gamma \leq 0.1$ for a fixed system size $L = 3000$. In the left panel of Fig. 3, we plot the $\gamma D_{LLG}(\rho, \gamma)$ as a function of the inverse persistence length $l_p^{-1} = \gamma$ ($v = 1$) for various $\rho = 0.01$ (blue square), 0.05 (red circle), 0.1 (black up-triangle) and 0.5 (magenta down-triangle). We observe the scaled bulk-diffusion coefficient $\gamma D_{LLG}(\rho, \gamma)$ to be a nonmonotonic function of the inverse persistence length γ and the nonmonotonicity effect is more pronounced at the lower density level. This nonmonotonicity is essentially due the intriguing interplay between persistence (induced by γ) and the hard-core repulsive interaction (governed by ρ). We also plot $\gamma D_{LLG}(\rho, \gamma)$ against ρ at the right panel of Fig. 3 for various $\gamma = 0.001$ (blue square), 0.005 (red circle), 0.01 (black up-triangle), 0.05 (magenta down-triangle) and 0.1 (green tilted square). Similar to the RTPs shown in Fig. (6b), we observe $\gamma D_{LLG}(\rho, \gamma)$ is a decreasing function of density ρ and as one increases the inverse persistence length γ , it shows a crossover from $1/\rho^2$ to $1/\rho$.

B. Verification of the scaling form of gap distribution $P(g)$

In this section, we numerically verify the assumed exponential form of the gap distribution $P(g)$ (see the paragraph between Eqs. (5) and (6) in the main text)

$$P(g) \simeq N_* \exp(-g/g_*), \quad (22)$$

along with the following scaling relation satisfied by the typical gap size g_*

$$g_* = \frac{1}{\rho} \mathcal{G}(\psi), \quad (23)$$

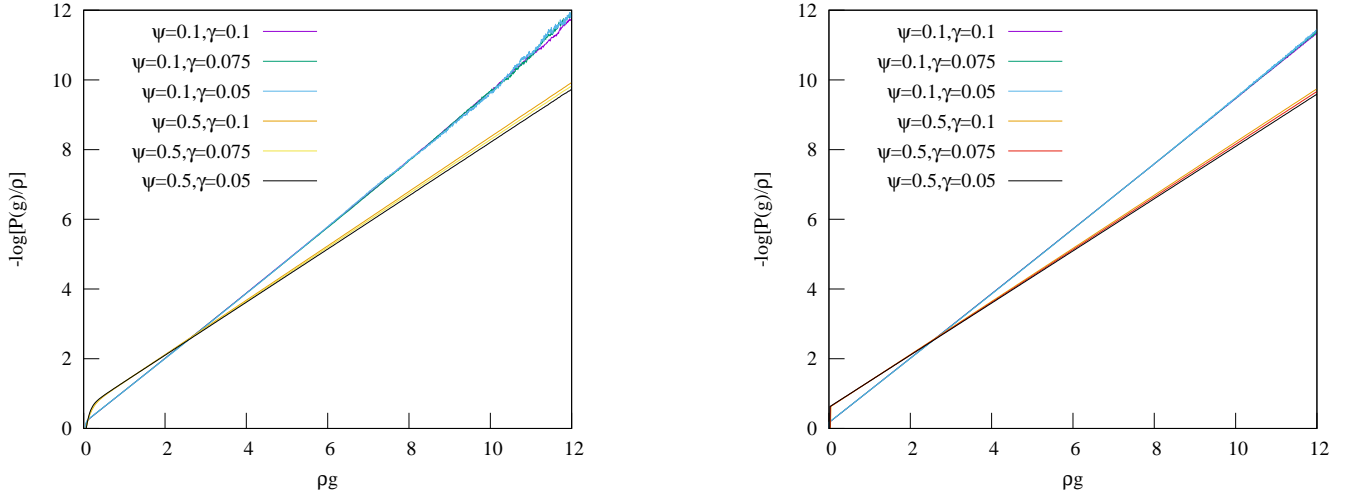


FIG. 4. *Verification of Eq. (25)*. We plot $-\ln(P(g)/\rho)$ as a function of ρg for RTPs (left-panel) and LLG model (right-panel) in $1D$, for various combinations of ρ and γ such that the scaling variable ψ remains fixed at 0.1 and 0.5. In both these panels, for $\psi = 0.1$, we have used $\gamma = 0.1$ (magenta line), 0.05 (green line) and 0.01 (sky blue line); while the same for $\psi = 0.5$ are shown in orange line, black line and blue line respectively.

for the LLG model and RTPs. Using the conservation law $\langle g \rangle = \sum_{g=1}^{\infty} gP(g) = 1/\rho$, which is exact in the low density limit, we trivially obtain the proportionality constant

$$N_* = \frac{1}{\rho} \frac{[\exp(\rho/\mathcal{G}(\psi)) - 1]^2}{\exp(\rho/\mathcal{G}(\psi))}. \quad (24)$$

We now insert g_* and N_* , as shown in Eq. (23) and (24), in the expression of $P(g)$, defined in Eq. (22) and obtain the scaling relation for $P(g)$,

$$-\ln\left(\frac{P(g)}{\rho}\right) = \frac{\rho g}{\mathcal{G}(\psi)} + 2\ln(\mathcal{G}(\psi)). \quad (25)$$

The above scaling relation is clearly a direct result of the assumed scaling form of g_* , as shown in Eq. (23). As a result, verifying Eq. (25) yields the existence of the proposed scaling relation of g_* right away. To do so, we compute and plot $P(g)$ for RTPs (left panel) and the LLG model (right panel) in $1D$ at various tumbling rates γ (various persistent length for LLG) and densities ρ , while keeping the ratio $\psi = \rho v/\gamma$ constant.

We plot $-\ln(P(g)/\rho)$ as a function of the scaled gap size ρg in Fig.(4) for two different $\psi = 0.1$ and 0.5. We obtain data for three different tumbling rates $\gamma = 0.05, 0.075$, and 0.1 for each ψ , and the corresponding density ρ is chosen from the relation $\rho = \gamma\psi/v$ (where $v = 1$). As shown in the figure, data belonging to different parameter spaces (ρ, γ) corresponding to the same ψ collapse quite well, indicating the validity of the assumed form of g_* , and the slope of the collapsed data is a measure of $1/\mathcal{G}(\psi)$.

C. Derivation of scaling function $\mathcal{F}_{LLG}(\psi)$ of the bulk-diffusion coefficient in the LLG

In this section, we derive the analytic expressions for the bulk-diffusivity $D_{LLG}(\rho, \gamma)$ and the corresponding scaling function $\mathcal{F}_{LLG}(\psi)$, presented in the main text in Eq. (6). We use the gap distribution function given in Eq. (22) and use it in Eq (21) in the limit of small γ and ρ , and obtain

$$D_{LLG}(\rho, \gamma) = -\frac{1}{2d} \frac{\partial}{\partial \rho} \left[N_* \rho \sum_{l=1}^{\infty} \phi(l) \left(\sum_{g=1}^{\infty} g e^{-g/g_*} + (l-1) \sum_{g=l}^{\infty} (g-l) e^{-g/g_*} \right) \right]. \quad (26)$$

Now, using the following identities,

$$\sum_{g=1}^{\infty} g e^{-g/g_*} = \frac{e^{1/g_*}}{(e^{1/g_*} - 1)^2} = \frac{1}{N_* \rho}, \quad (27)$$

$$\sum_{g=l}^{\infty} (g-l) e^{-g/g_*} = \frac{e^{-(l-1)/g_*}}{(e^{1/g_*} - 1)^2} = \frac{e^{-l/g_*}}{N_* \rho}, \quad (28)$$

$$\phi(l) = \frac{1}{l_p} e^{-l/l_p} = \frac{\gamma}{v} e^{-\gamma l/v}, \quad (29)$$

we can rewrite and simplify Eq. (26) as

$$D_{LLG}(\rho, \gamma) = -\frac{\gamma}{2vd} \frac{\partial}{\partial \rho} \left[\sum_{l=1}^{\infty} e^{-\gamma l/v} + \sum_{l=1}^{\infty} (l-1) e^{-(\gamma/v+1/g_*)l} \right]. \quad (30)$$

Note that, the first term inside the square bracket of Eq. (30) is independent of ρ and vanishes upon differentiation. On the other hand, the summation appearing in the second term is given by,

$$\sum_{l=1}^{\infty} (l-1) e^{-(\gamma/v+1/g_*)l} = \frac{1}{(e^{(\gamma/v+1/g_*)} - 1)^2}. \quad (31)$$

We now use the scaling form of g_* as given in Eq. (23) and calculate,

$$\frac{\partial g_*}{\partial \rho} = -\frac{g_*}{\rho} \left(1 - \psi \frac{\mathcal{G}'(\psi)}{\mathcal{G}(\psi)} \right). \quad (32)$$

Finally, substituting all the results defined above in Eq. (30), the bulk-diffusion coefficient can be written as,

$$D_{LLG}(\rho, \gamma) = \frac{\gamma e^{(\gamma/v+\rho/\mathcal{G}(\psi))}}{vd\mathcal{G}(\psi)(e^{(\gamma/v+\rho/\mathcal{G}(\psi))} - 1)^3} \left(1 - \psi \frac{\mathcal{G}'(\psi)}{\mathcal{G}(\psi)} \right). \quad (33)$$

Asymptotic expansion of $D_{LLG}(\rho, \gamma)$: We further expand the bulk-diffusion coefficient $D_{LLG}(\rho, \gamma)$, obtained in Eq. (33), in the limit of $\gamma \rightarrow 0$ and $\rho \rightarrow 0$, such that the dimensionless quantity $\psi = \rho v/\gamma$ remains finite. Let us first make the replacement,

$$n = \frac{\gamma}{v} + \frac{\rho}{\mathcal{G}(\psi)} \equiv \frac{\gamma}{v} \left(1 + \frac{\psi}{\mathcal{G}(\psi)} \right). \quad (34)$$

Note that this particular limit of interest automatically implies $n \rightarrow 0$. We now expand the following expression as

$$\begin{aligned} \frac{\gamma e^n}{v(e^n - 1)^3} &= \frac{\gamma \left(1 + n + \frac{n^2}{2} \dots \right)}{vn^3 \left(1 + \frac{n}{2} + \frac{n^2}{6} \dots \right)^3} \\ &\simeq \frac{\gamma}{v} \left(\frac{1}{n^3} - \frac{1}{2n^2} - \frac{3}{2n} \dots \right). \end{aligned} \quad (35)$$

Since we are working in the regime $n \rightarrow 0$, the leading order contribution to Eq. (35) emerges from $1/n^3$ term only and consequently the bulk-diffusion coefficient can be written as

$$\begin{aligned} D_{LLG}(\rho, \gamma) &= \frac{\gamma}{v d n^3 \mathcal{G}(\psi)} \left(1 - \psi \frac{\mathcal{G}'(\psi)}{\mathcal{G}(\psi)} \right) + \mathcal{O}\left(\frac{\gamma}{n^2}\right), \\ &\simeq \frac{v^2 \mathcal{G}^2(\psi)}{\gamma^2 d (\mathcal{G}(\psi) + \psi)^3} \left(1 - \psi \frac{\mathcal{G}'(\psi)}{\mathcal{G}(\psi)} \right) + \mathcal{O}\left(\frac{1}{\gamma}\right). \end{aligned} \quad (36)$$

From the above equation, it is quite evident that $D_{LLG}(\rho, \gamma)$ satisfies a scaling relation and the corresponding scaling function can be written as

$$\mathcal{F}_{LLG}(\rho, \gamma) = \frac{1}{d} \left(\frac{\gamma}{v} \right)^2 D_{LLG}(\rho, \gamma) \simeq \frac{\mathcal{G}^2(\psi)}{(\mathcal{G}(\psi) + \psi)^3} \left(1 - \psi \frac{\mathcal{G}'(\psi)}{\mathcal{G}(\psi)} \right). \quad (37)$$

D. Numerical scheme to calculate the bulk-diffusion coefficients for Run-and-Tumble particles (RTPs)

We now provide the details of the simulation scheme [57], used in the main text to calculate the bulk-diffusion coefficient $D_{RTP}(\rho, \gamma)$ from arbitrary density and tumbling rate. According to the scheme, we create an initial slowly varying sinusoidal density perturbation as given in Eq. (38); the density perturbation relaxes with time and measuring the relaxation rate directly from simulations helps us calculate the bulk-diffusivity of the system. We let the system evolve from an initial density perturbation applied along one direction while maintaining a uniform density profile across all other $d - 1$ directions. The initial density perturbation in this case is given by,

$$\delta\rho(x, 0) = \rho(x, 0) - \rho_0 = A(0) \sin(2\pi x), \quad (38)$$

where ρ_0 is the uniform background density over which the perturbation is applied. On the coarse-grained scale i.e. $x = X/L$ and $\tau = t/L^2$ (here t is unscaled microscopic time for RTPs), the system is assumed to overcome the ballistic relaxation mode due to inherent persistence (we verify this in Sec. E) and consequently the density field $\rho(x, \tau)$ evolves according to the diffusion equation,

$$\frac{\partial\rho(x, \tau)}{\partial\tau} = \frac{\partial}{\partial x} \left[D_{RTP}(\rho, \gamma) \frac{\partial\rho(x, \tau)}{\partial x} \right], \quad (39)$$

which in general is a nonlinear equation and is difficult to solve exactly for arbitrary τ . However, in the limit of small perturbation, i.e. $A(0) \ll \rho_0$, we can write $D_{RTP}[\rho(x, \tau), \gamma] \simeq D_{RTP}(\rho_0, \gamma)$ and consequently Eq. (39) becomes linear, i.e.,

$$\frac{\partial\rho(x, \tau)}{\partial\tau} = D_{RTP}(\rho_0, \gamma) \frac{\partial^2\rho(x, \tau)}{\partial x^2}, \quad (40)$$

which admits the following solution,

$$\delta\rho(x, \tau) = \rho(x, \tau) - \rho_0 = A(\tau) \sin(2\pi x). \quad (41)$$

Here the amplitude $A(\tau)$ is given by

$$A(\tau) = A(0)e^{-4\pi^2 D_{RTP}(\rho_0, \gamma)\tau} \equiv A(0)e^{-\Gamma(\rho_0, \gamma)\tau} \quad (42)$$

and the relaxation rate is related to the bulk-diffusion coefficient as

$$\Gamma(\rho, \gamma) = 4\pi^2 D_{RTP}(\rho, \gamma). \quad (43)$$

Note that, the relaxation rate Γ is a function of density ρ as well as the tumbling rate γ . In simulations, we calculate the excess number of particles in the first half of the system $\Delta(\tau)$, which is directly related with the amplitude $A(\tau)$: $\Delta(\tau) = L^d \int_0^{1/2} \delta\rho(x, \tau) dx = L^d \pi A(\tau)$. Upon obtaining $\Delta(\tau)$ (hence $A(\tau)$) at various τ , we measure the relaxation rate and obtain the bulk-diffusion coefficient from the relation $D_{RTP} = \Gamma/4\pi^2$. As the characterization of collective diffusion is the focal point of our work, we require the system to reach the diffusive regime. We ensure this by evolving the system upto $t \sim L^2$, where L is large implying the relaxation of long wavelength mode. In this process, we take the system size limit $L \gg 1$ first and then varying the tumbling rate γ carefully, so that the persistent length $l_p = \gamma^{-1}$ (where $v = 1$) always remains much smaller than L , i.e. $l_p \ll L$. We have done the analysis for $L = 3000$ and the averaging were done over 10^4 realizations. In Fig. 5, we have shown the time dependence of the perturbation amplitude $A(\tau)$, which indeed shows exponential decay as in Eq. (42). Calculating the slope of decay in semi-log scale, the relaxation rate Γ is estimated, which according to Eq. (43), gives the bulk-diffusion coefficient $D_{RTP}(\rho, \gamma)$ of the system.

In the left panel of Fig. (6), we plot the unscaled bulk-diffusion coefficient $D_{RTP}(\rho, \gamma)$ as a function of tumbling rate γ at various densities $\rho = 0.01$ (blue square), 0.05 (red circle), 0.1 (black upper-triangle), 0.5 (magenta lower-triangle). At large γ , we observe $D_{RTP}(\rho, \gamma)$ to be independent of both ρ and γ and approaches to a constant value $1/2$ which is expected, as in this limit, particles randomly flip their orientation and the RTP dynamics essentially transforms into the well-known symmetric simple exclusion process (SSEP) in which case the diffusion coefficient is indeed $1/2$ at all densities. On the other hand, at small γ , particles tend to move persistently along the same direction up to time $\tau_p = 1/\gamma \gg 1$, which enhances diffusion. However, the free propagation of persistently moving particles gets obstructed by the presence of another particle in the direction of motion due to hardcore repulsion, which restricts particles to diffuse. Therefore, persistence and hard-core repulsion act in the opposite sense and the interplay between them essentially leads to nonmonotonic variation of bulk-diffusion coefficient $D_{RTP}(\rho, \gamma)$ in tumbling rate γ . When

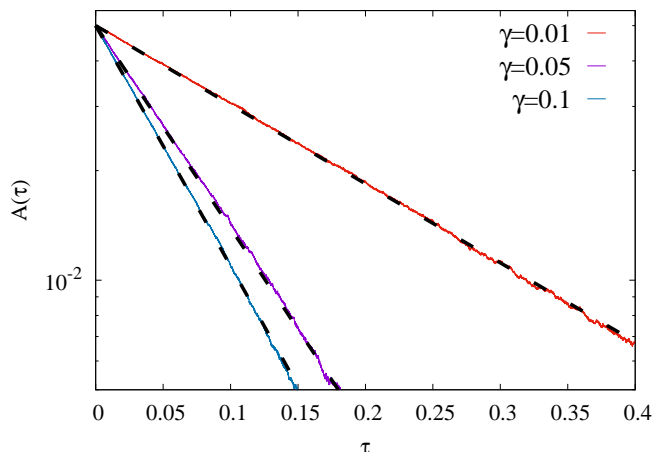


FIG. 5. We have plotted perturbation amplitude $A(\tau)$, as a function of the hydrodynamic time τ , for tumbling rates $\gamma = 0.01$ (red line), 0.05 (magenta line) and 0.1 (blue line), while the black dotted lines are the best fitted data, which according to Eq. (42), we obtain relaxation rates $\Gamma = 5, 12.8$ and 15.2 for $\gamma = 0.01, 0.05$ and 0.1 respectively. For both these panels, we have fixed $\rho = 0.5$ and $A(0) = \rho_0/10 = 0.05$.

the mean gap size $\langle g \rangle = \rho^{-1}$ is larger than the persistent length γ^{-1} , particles barely feel the presence of others and the persistence effect dominates over hard-core repulsion, which in turn increases the bulk-diffusion coefficient $D_{RTP}(\rho, \gamma)$ with decreasing γ . Keeping ρ fixed at a finite value, when one decreases γ further and reaches the opposite limit i.e. $\rho^{-1} < \gamma^{-1}$, the hardcore repulsion dominates over persistence and two oppositely moving particles upon collision block each other's movement. Since spin flipping time is quite large in this limit, by the time one of them reorient its direction to restart their journey, many other particles approach them from both the directions and eventually particles are trapped inside a cluster with two boundary particles orienting themselves towards the cluster, which significantly reduces $D_{RTP}(\rho, \gamma)$ of the system. In such case, diffusion takes place only when one of the boundary particles from a cluster flips and, as we know local spin-flipping event takes place at a time scale $1/\gamma$, we expect the bulk-diffusion coefficient $D_{RTP}(\rho, \gamma) \sim \gamma$ for very small tumbling rate γ . The right panel of Fig. (6) shows the variation of $D_{RTP}(\rho, \gamma)$ with ρ at different $\gamma = 0.001$ (blue square), 0.005 (red circle), 0.01 (black upper-triangle), 0.05 (magenta lower-triangle) and 0.1 (green tilted-square). Unlike the previous scenario, in this case $D_{RTP}(\rho, \gamma)$ is observed to be a monotonically decreasing function of ρ . For a fixed γ , as one increases ρ , the typical gap size $\langle g \rangle = 1/\rho$ is reduced and hence hard-core repulsion effect dominates over persistent motion of particles and as before $D_{RTP}(\rho, \gamma)$ decreases.

E. Verification of the existence of diffusive scaling limit for RTPs

One of the central assumptions in calculating $D_{RTP}(\rho, \gamma)$ is that the long wavelength relaxation is only dominated by the diffusive modes and consequently the time evolution of the density field $\rho(X, t)$ can be described by the diffusion equation, i.e., on a coarse-grained scale the system should satisfy diffusive scaling: $\rho(X, t) \equiv \rho(X/L, t/L^2)$, $J(X, t) \equiv L^{-1}J(X/L, t/L^2)$. Here we want to verify the existence of such scaling for RTPs. For this purpose, we study the relaxation of the density field $\rho(x, \tau)$ as a function of scaled position $x = X/L$ for different system sizes L and different microscopic times t such that the hydrodynamic time $\tau = t/L^2$ remains fixed. The scaling limit would be verified if different curves corresponding to different L at the same τ collapse with each other and the collapsed data must be the solution of the nonlinear diffusion equation Eq. (39).

To verify the diffusive scaling limit, we simulate the model in $1D$ with a slowly varying sinusoidal density profile over a uniform background as defined in Eq. (38). In Fig. (E), we plot the scaled excess density field $\delta\rho(x, \tau) = \rho(x, \tau) - \rho_0$, obtained from simulation, as a function of the scaled position $x = X/L$, at different hydrodynamic time $\tau = 0.1$ (left panel) and 0.2 (right panel), for different system sizes $L = 1000$ (blue square), 2000 (magenta triangle) and 3000 (red circle) at $\gamma = 0.01$ and 0.005 respectively. Throughout the analysis, we have fixed the background density at $\rho_0 = 0.5$ and averaging are done over 10^4 realizations. We also numerically integrate Eq. (39) using the initial condition defined in Eq. (38) and the corresponding solution is plotted in black solid line. We observe the simulation points along with the analytic solution collapse quite well and hereby assert the existence of diffusive scaling limit for RTPs.

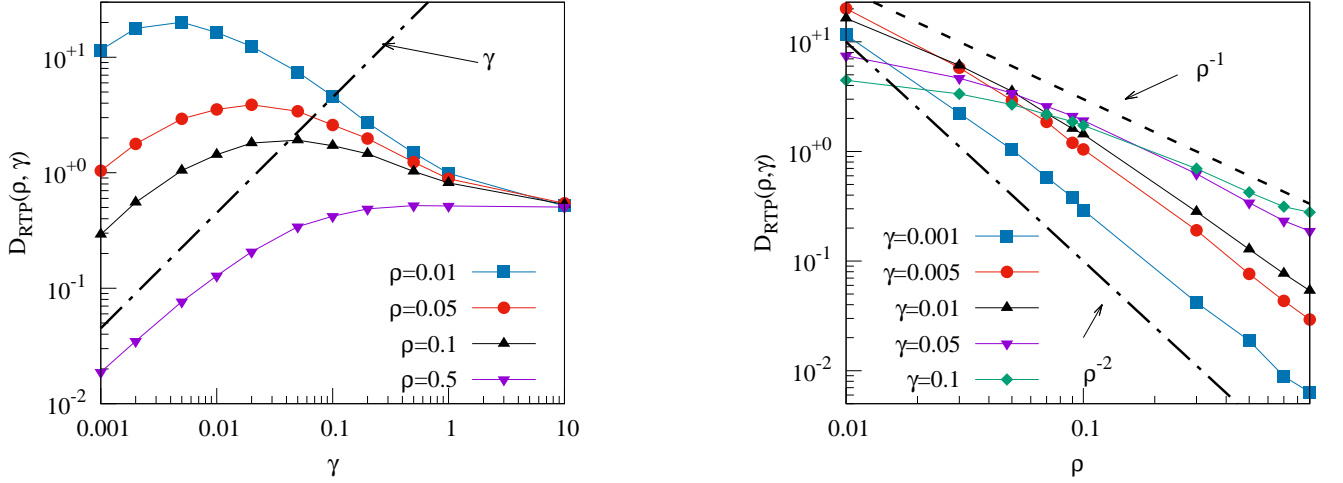


FIG. 6. *Bulk-diffusion coefficient for run-and-tumble particles.* In the left panel, we plot $D_{RTP}(\rho, \gamma)$ as a function of spin-flipping rate γ for various density $\rho = 0.01$ (blue square), 0.05 (red circle), 0.1 (black up-triangle), 0.5 (magenta down-triangle), while in the right panel, $D_{RTP}(\rho, \gamma)$ is plotted against density ρ for different spin-flipping rate $\gamma = 0.001$ (blue square), 0.005 (red circle), 0.01 (black up-triangle), 0.05 (magenta down-triangle) and 0.1 (green tilted square).

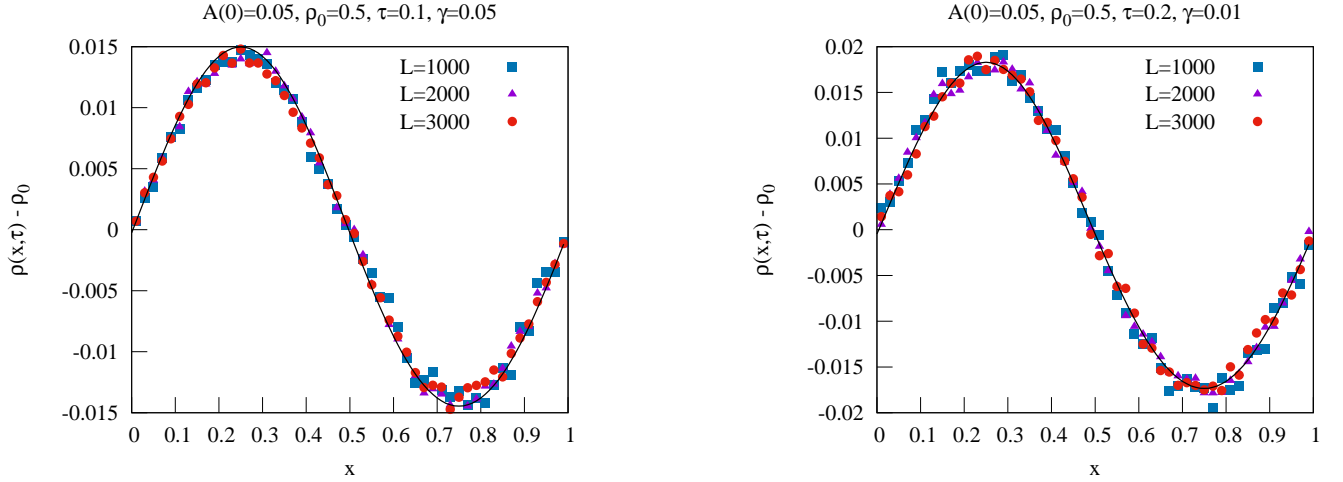


FIG. 7. *Verification of diffusive scaling.* In the left panel, we plot the excess density field $\delta\rho(x, \tau) = \rho(x, \tau) - \rho_0$ for $\gamma = 0.05$, obtained from simulation, as a function of the scaled position $x = X/L$ at different microscopic times $t = 1 \times 10^5$ for $L = 1000$ (blue square), $t = 4 \times 10^5$ for $L = 2000$ (magenta up-triangle) and $t = 9 \times 10^5$ for $L = 3000$ (red circle) such that the hydrodynamic time is fixed at $\tau = t/L^2 = 0.1$, while in the right panel, we plot the same for $\gamma = 0.01$ at $t = 2 \times 10^5$ for $L = 1000$ (blue square), $t = 8 \times 10^5$ for $L = 2000$ (magenta up-triangle) and $t = 1.8 \times 10^6$ for $L = 3000$ (red circle) such that the hydrodynamic time is fixed at $\tau = t/L^2 = 0.2$. In both the cases we relax the system with a sinusoidal initial condition defined in Eq. (38) with $\rho_0 = 0.5$. Corresponding lines are obtained by numerically integrating the hydrodynamic equation using the bulk-diffusion coefficient obtained from simulation. For both the γ values, density profiles corresponding to same τ for different L collapse quite well.

F. Verification of hydrodynamics through density relaxation

In this section, we further verify the hydrodynamic description, as shown in Eq. (39), by relaxing the initial density perturbation through the already obtained bulk-diffusion coefficients $D_{RTP}(\rho, \gamma)$ and $D_{LLG}(\rho, \gamma)$ for RTPs and LLG respectively. As mentioned above, on the coarse grained scale, i.e., $x = X/L$ and $\tau = t/L^2$, the density relaxation is governed by the non-linear diffusion equation Eq. (39) and we can compare the exact numerical solution of Eq. (39) (obtained through Euler integration method) and compare with simulations. For this purpose, we take the initial density perturbation to be a step-function with step height ρ_1 and width w over a uniform background density ρ_0 ,

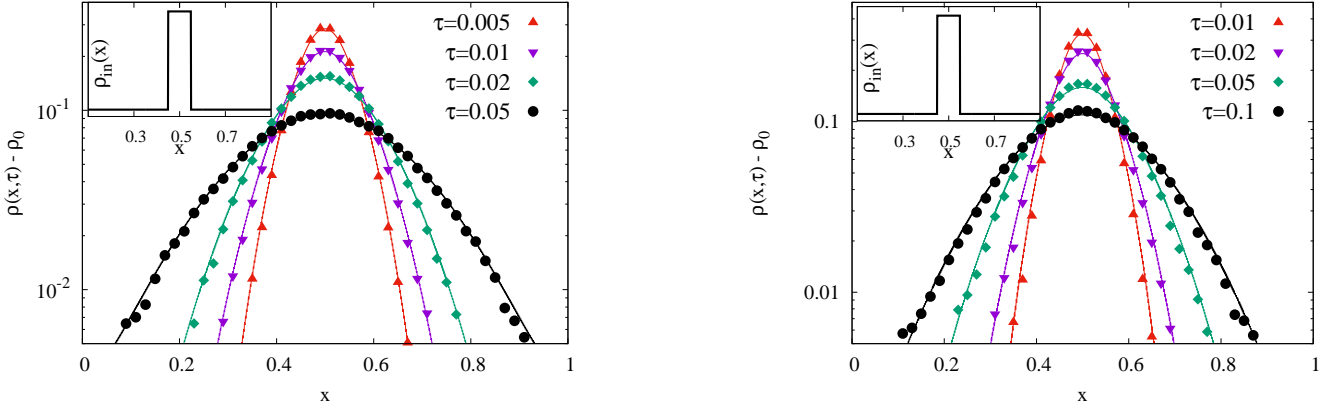


FIG. 8. *Verification of bulk-diffusion coefficient $D_{RTP}(\rho, \gamma)$.* We verify the bulk-diffusion coefficient $D_{RTP}(\rho, \gamma)$ through the relaxation from an initial density perturbation, defined in Eq. (44), at various hydrodynamic times τ . In the left-panel, we plot the numerically obtained excess density profile $\delta\rho(x, \tau) = \rho(x, \tau) - \rho_0$ for $\gamma = 0.05$ as a function of the scaled position x at $\tau = 0.005$ (red up-triangle), 0.01 (magenta down-triangle), 0.02 (green tilted square), 0.05 (black circle). In the right-panel we plot the same for $\gamma = 0.01$ at $\tau = 0.01$ (red up-triangle), 0.02 (magenta down-triangle), 0.05 (green tilted square) and 0.1 (black circle). Corresponding lines are the data obtained by integrating the hydrodynamic equation. For both the cases, we relax the system from same initial condition with $\rho_0 = 0.5$, $\rho_1 = 0.4$ and $w = 0.1$ and they are plotted at the inset of the respective panels.

which mathematically can be expressed as,

$$\rho(x, \tau = 0) = \begin{cases} \rho_0 + \rho_1 & \text{for } |x - \frac{1}{2}| \leq \frac{w}{2}, \\ \rho_0 & \text{otherwise.} \end{cases} \quad (44)$$

In Fig. 8 we plot the excess density field $\delta\rho(x, \tau) = \rho(x, \tau) - \rho_0$, obtained from simulation at two tumbling rates $\gamma = 0.05$ (left panel) and 0.01 (right panel), as a function of the coarse-grained space $x = X/L$ using the initial condition defined in Eq. (44) at different hydrodynamic times $\tau = 10^{-3}$ (red tilted-square), 2×10^{-3} (black up-triangle), 5×10^{-3} (magenta down-triangle) and the corresponding lines are obtained by numerically integrating Eq. (39) using our obtained diffusion coefficient $D_{RTP}(\rho, \gamma)$ with the same initial condition defined in Eq. (44). For both the panels, the result is obtained for $1D$ with $L = 1000$, $\rho_1 = 0.4$, $\rho_0 = 0.5$, $w = 0.1$ and averaging were done over 10^4 realizations. The simulation data matches quite well with the hydrodynamic theory, therefore the obtained diffusion coefficient $D_{RTP}(\rho, \gamma)$ is correct.

For the LLG model in $1D$, we proceed with $\rho_0 = 0.5$, $\rho_1 = 0.4$, $w = 0.1$ and the relaxation is studied for two different $\gamma = 0.05$ and 0.01, same as RTPs. In the left panel of Fig. 9, we plot the excess density field $\delta\rho(x, \tau)$, obtained from simulations, as a function of the scaled position x for $\gamma = 0.05$ at different hydrodynamic time $\tau = 0.001$ (blue square), 0.002 (red circle), 0.005 (black up-triangle), 0.01 (magenta down-triangle), while at the right panel, we plot the same for $\gamma = 0.01$ at $\tau = 0.002$ (blue circle), 0.005 (red up-triangle), 0.01 (black square), 0.02 (magenta down-triangle). We have done averaging over 10^4 realizations. To verify the hydrodynamic density evolution equation or the obtained bulk diffusion coefficient $D_{LLG}(\rho, \gamma)$, we perform Euler integration of Eq. (39) by using the initial condition defined in Eq. (44) for the same parameters defined above and plot the solutions as lines in both the panels of Fig. 9. For both the γ values, we observe a good match between the simulation data (points) and hydrodynamic theory (line).

G. Verification of emergent hydrodynamics

As discussed in the main text, in the limit of strong persistence i.e. $\gamma \rightarrow 0$, the unscaled bulk-diffusion coefficient $D_{RTP}(\rho, \gamma)$ shows anomalous behavior; in the low density limit, it diverges as $1/\gamma$, while in the finite density limit, it vanishes as $D_{RTP} \sim \gamma$. Furthermore, on the time scale of RTPs, the bulk-diffusion coefficient of the LLG model $\gamma D_{LLG}(\rho, \gamma)$, exhibits similar characteristics. Consequently, the hydrodynamic description is not meaningful in the limit $\gamma \rightarrow 0$. Therefore, to maintain an appropriate hydrodynamic structure, one cannot independently vary ρ and γ and, from the scaling relation satisfied by $D(\rho, \gamma)$, we see that proper hydrodynamics scaling is recovered only when we rescale the density field $\psi = \rho/\gamma$ and time $\tilde{\tau} = \tau/\gamma$ (for RTPs) and $\tilde{\tau} = \tau/\gamma^2$ (for LLG) and the corresponding hydrodynamic equation is given by,

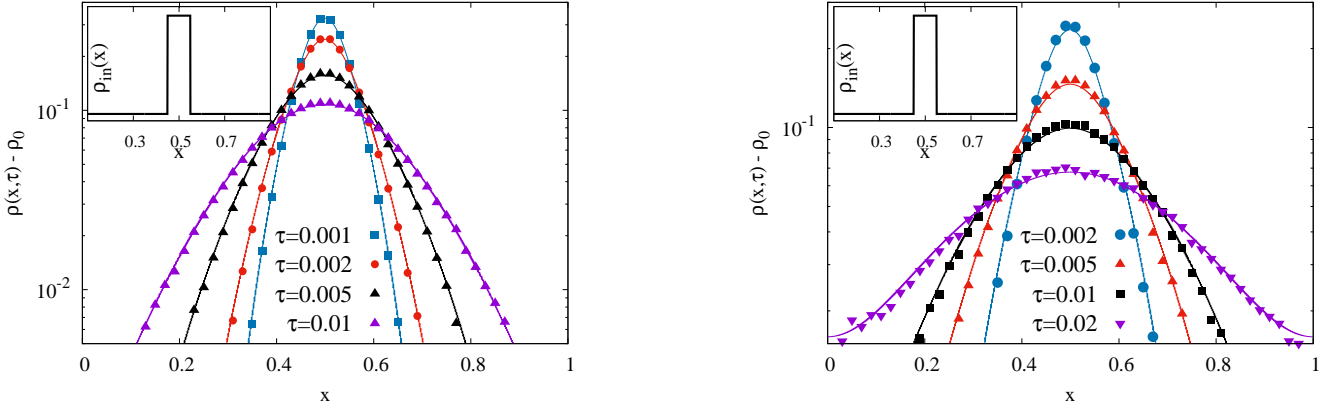


FIG. 9. *Verification of bulk-diffusion coefficient $D_{LLG}(\rho, \gamma)$.* We verify the bulk-diffusion coefficient $D_{LLG}(\rho, \gamma)$ through the relaxation from an initial density perturbation, defined in Eq. (44), at various hydrodynamic times τ . In the left-panel, we plot the numerically obtained excess density profile $\delta\rho(x, \tau) = \rho(x, \tau) - \rho_0$ for $\gamma = 0.05$ as a function of the scaled position x at $\tau = 0.001$ (blue square), 0.002 (red circle), 0.005 (black up-triangle) and 0.01 (magenta down-triangle). In the right-panel, we plot the same for $\gamma = 0.01$ at $\tau = 0.002$ (blue circle), 0.005 (red up-triangle), 0.01 (black square) and 0.02 (magenta down triangle). Corresponding lines are the data obtained by integrating the hydrodynamic equation. For both the cases, we relax the system from same initial condition with $\rho_0 = 0.5$, $\rho_1 = 0.4$ and $w = 0.1$ and they are plotted at the inset of the respective panels.

$$\frac{\partial\psi(x, \tilde{\tau})}{\partial\tilde{\tau}} = \frac{\partial}{\partial x} \left[\mathcal{F}(\psi) \frac{\partial\psi(x, \tilde{\tau})}{\partial x} \right]. \quad (45)$$

To verify Eq. (45), in Fig. (10) we plot the scaled density field $\psi(x, \tilde{\tau}) = \rho(x, \tau = \tilde{\tau}\gamma)/\gamma$ for RTPs (left panel) and $\rho(x, \tau = \tilde{\tau}\gamma^2)/\gamma$ for LLG (right panel) as a function of coarse-grained position $x = X/L$ for different spin-flipping rate γ and hydrodynamic time τ while keeping the rescaled time remain fixed at $\tilde{\tau} = \tau/\gamma$ for RTPs and τ/γ^2 for LLG. Different curves corresponding to different γ at the same $\tilde{\tau}$ are expected to collapse with each other and the collapsed profile at different $\tilde{\tau}$ should be governed by the solution of the nonlinear diffusion equation Eq. (45). We choose the initial scaled density profile $\psi(x, \tilde{\tau} = 0)$ to be a step function with step height ψ_1 and width w over a uniform background profile ψ_0 , i.e.

$$\psi(x, \tilde{\tau} = 0) = \begin{cases} \psi_0 + \psi_1 & \text{for } |x - \frac{1}{2}| \leq \frac{w}{2}, \\ \psi_0 & \text{otherwise.} \end{cases} \quad (46)$$

For a fixed γ , we prepare a step profile for the density field $\rho(x, 0)$ with step height ρ_1 and width w around $x = 1/2$ over a uniform background density ρ_0 such that the rescaled density $\psi_0 = \rho_0/\gamma$ and $\psi_1 = \rho_1/\gamma$ remain fixed for all γ . In Fig. 10, for a fixed $\psi_0 = 40$ and $\psi_1 = 40$, we plot the relaxation of the excess rescaled density field $\psi(x, \tilde{\tau}) - \psi_0$, obtained from simulation, as a function of x for different $\gamma = 0.01$ (open symbols) and 0.005 (closed symbols) at various rescaled hydrodynamic time $\tilde{\tau} = 5$ (red line), 10 (blue line) and 20 (magenta line) for RTPs (left panel) and $\tilde{\tau} = 40$ (red line), 80 (blue line) and 160 (magenta line) for LLG (right panel) and the corresponding lines are the results obtained from numerical integration of Eq. (45) with the same initial condition using numerically obtained $\mathcal{F}_{RTP}(\psi)$ for RTPs and $\mathcal{F}_{LLG}(\psi)$ for LLG as given in Eq. (7) in the main text. Simulation and analytical data corresponding to these two different γ values are observed to collapse quite well for both these models, which consequently verifies the existence of the proper hydrodynamic equation Eq. (45).

H. Power-law dependence of the bulk-diffusion coefficient

In the main text, we have characterized the superdiffusive (ballistic) collective transport of active particles for $\gamma = 0.05$. The scaling relation is obtained by assuming the $1/\rho$ dependence of the bulk-diffusion coefficient $D(\rho, \gamma)$. To support this assumption, in Fig. 11, we present the density dependence of the numerically obtained $D(\rho, \gamma)$ for RTPs (left-panel) and the LLG model (right-panel). We observe over a broad range in density, $D(\rho, \gamma)$ obeys $1/\rho$ scaling which is shown here by the solid black line.

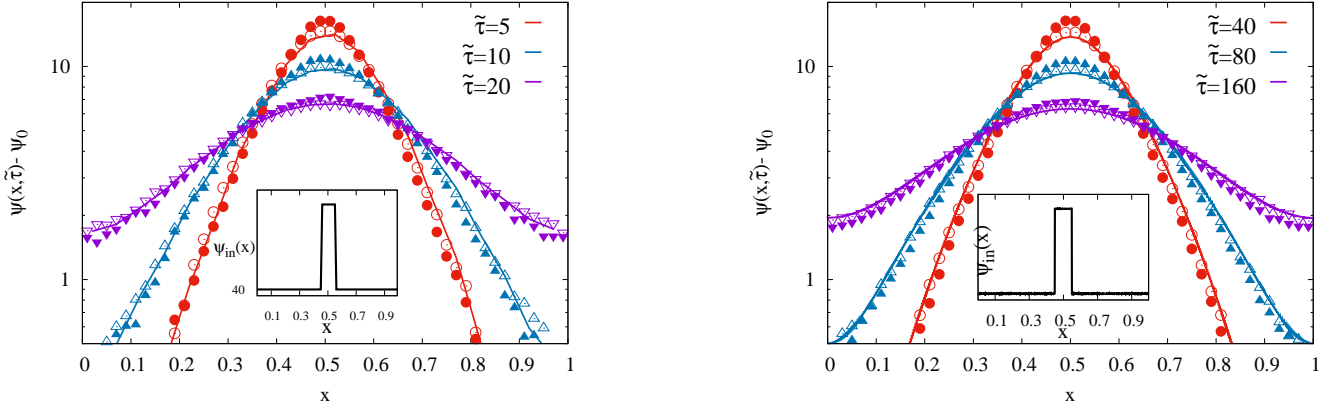


FIG. 10. *Relaxation of scaled density field* $\psi(x, \tilde{\tau})$. We plot the scaled excess density field $\delta\psi(x, \tilde{\tau}) = \psi(x, \tilde{\tau}) - \psi_0$, for RTPs (left-panel) and the LLG model (right-panel), as a function of the scaled position x at various rescaled time $\tilde{\tau}$ for two different $\gamma = 0.005$ and 0.01 . In case of $\gamma = 0.005$, we numerically obtain excess density profiles $\delta\rho(x, \tau)$ with $\rho_0 = 0.2$, $\rho_1 = 0.2$ at hydrodynamic times $\tau = 2.5 \times 10^{-2}$ (red filled circle), 5×10^{-2} (blue filled up-triangle), 1×10^{-1} (magenta filled down-triangle) (for RTPs) and $\tau = 10^{-3}$ (red filled circle), 2×10^{-3} (blue filled up-triangle), 4×10^{-3} (magenta filled down-triangle) (for LLG model); while the corresponding parameters for $\gamma = 0.01$ are $\rho_0 = 0.4$, $\rho_1 = 0.4$, $\tau = 5 \times 10^{-2}$ (red open circle), 1×10^{-1} (blue open up-triangle), 2×10^{-1} (magenta open down-triangle) (for RTPs) and $\tau = 4 \times 10^{-3}$ (red open circle), 8×10^{-3} (blue open up-triangle), 1.6×10^{-2} (magenta open down-triangle) (for LLG) such that the rescaled variables are fixed at $\psi_0 = \rho_0/\gamma = 40$, $\psi_1 = \rho_1/\gamma = 40$ and $\tilde{\tau} = \tau/\gamma^2 = 5, 10, 20$ (for RTPs) and $40, 80, 160$ (for LLG). Corresponding lines are obtained by integrating Eq. (45) using the scaling function $\mathcal{F}_{RTP}(\psi)$ obtained from simulation and $\mathcal{F}_{LLG}(\psi)$ from Eq. (7) in main text. We observe a good collapse between simulation points and a reasonably good agreement with theory (lines).

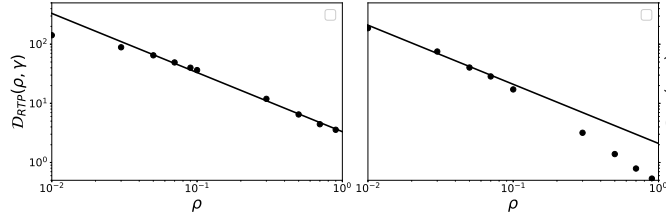


FIG. 11. We plot the scaled bulk-diffusion coefficients $D_{RTP}(\rho, \gamma)$ and $D_{LLG}(\rho, \gamma)$ as a function of ρ for RTPs (left-panel) and LLG (right-panel), respectively; guiding lines represent the power-law form C/ρ which was used to derive the scaling function $\mathcal{R}(\xi)$ in Eq. (14) and where the values of C depend on the microscopic details of the model - $C = 3.32$ for RTPs and $C = 2.2$ for LLG model respectively. Here note that, for RTPs the scaled bulk-diffusion coefficient is $\mathcal{D}_{RTP} \equiv D_{RTP}/\gamma$ and for LLG $\mathcal{D}_{LLG} \equiv D_{LLG}$.

I. Calculation of the scaling function $\mathcal{R}(\xi)$

In this section, we will show quantitatively how power-law density dependence in bulk-diffusion coefficient leads to anomalous scaling in collective transport, as discussed in the main text. For this purpose, the most general expression of the bulk-diffusion coefficient can be written as

$$D(n) \simeq \frac{C}{\rho^\alpha}, \quad (47)$$

where the coefficient C and the exponent α depend on the specific model considered. The corresponding evolution equation of the microscopic density $\rho(X, t)$ is given by,

$$\frac{\partial \rho(X, t)}{\partial t} = C \frac{\partial}{\partial X} \left(\frac{1}{\rho^\alpha} \frac{\partial \rho}{\partial X} \right), \quad (48)$$

where X and t are the space and time coordinates, respectively, at the microscopic scale. In order to solve the above equation, from an initially localized distribution $\rho(X, 0) = \rho_1 \delta(X)$, we proceed with the following scaling ansatz,

$$\rho(X, t) = \frac{1}{(Ct)^\omega} \mathcal{R} \left(\frac{X}{(Ct)^\omega} \right), \quad (49)$$

where $\xi = X/(Ct)^\omega$ is the scaling variable. Note that, the growth exponent ω essentially characterizes the anomaly in the collective transport; $\omega = 1/2$ corresponds to normal diffusive transport, while $\omega > 1/2$ and $\omega < 1/2$ indicate the transport to be superdiffusive and subdiffusive respectively. Finally, plugging the above scaling solution in Eq. (48), we obtain

$$\omega \frac{d(\xi \mathcal{R})}{d\xi} = - (Ct)^{1-(2-\alpha)\omega} \frac{d}{d\xi} \left[\mathcal{R}^{-\alpha} \frac{d\mathcal{R}}{d\xi} \right]. \quad (50)$$

However, to exhibit self-similar solution, Eq. (50) should not contain t explicitly, implying $1 - (2 - \alpha)\omega = 0$, or

$$\omega = \frac{1}{2 - \alpha}. \quad (51)$$

Eq. (51) directly relates the growth exponent ω to the exponent α and is displayed in the main text.

We note that, depending on the parameter regime the exponent α lies in the range $0 \leq \alpha \leq 2$. Now, to demonstrate Eq. (48) and Eq. (50), we choose a particularly interesting regime for which $\alpha = 1$ and, from Eq. (51), it immediately implies $\omega = 1$. This indicates the model should exhibit *ballistic* transport. In this particular regime, $\mathcal{R}(\xi)$ obeys the following equation,

$$\frac{d(\xi \mathcal{R})}{d\xi} = - \frac{d^2}{d\xi^2} [\ln \mathcal{R}]. \quad (52)$$

By using the boundary condition $d\mathcal{R}/d\xi = 0$ for $\xi = 0$ (source free solution), the above equation reduces to

$$\frac{d \ln \mathcal{R}}{d\xi} = -\xi \mathcal{R}. \quad (53)$$

We further use another boundary condition $\mathcal{R}(\xi = 0) = \xi_0^2/2$, which immediately implies the solution to be,

$$\mathcal{R}(\xi) = \frac{2}{\xi_0^2 + \xi^2}. \quad (54)$$

The above solution is the desired scaling function which we have shown in the main text.

- [1] M. C. Marchetti, J. F. Joanny, S. Ramaswamy, T. B. Liverpool, J. Prost, M. Rao, and R. A. Simha, *Rev. Mod. Phys.* **85**, 1143 (2013).
- [2] X.-L. Wu and A. Libchaber, *Phys. Rev. Lett.* **84**, 3017 (2000).
- [3] B. Wang, S. M. Anthony, S. C. Bae, and S. Granick, *Proceedings of the National Academy of Sciences* **106**, 15160 (2009) <https://www.pnas.org/doi/pdf/10.1073/pnas.0903554106>.
- [4] K. C. Leptos, J. S. Guasto, J. P. Gollub, A. I. Pesci, and R. E. Goldstein, *Phys. Rev. Lett.* **103**, 198103 (2009).
- [5] A. Kudrolli, *Phys. Rev. Lett.* **104**, 088001 (2010).
- [6] B. Wang, J. Kuo, S. C. Bae, and S. Granick, *Nature Materials* **11**, 481 (2012).
- [7] G. Ariel, A. Rabani, S. Benisty, J. D. Partridge, R. M. Harshey, and A. Be'Er, *Nature communications* **6**, 1 (2015).
- [8] H. M. López, J. Gachelin, C. Douarche, H. Auradou, and E. Clément, *Phys. Rev. Lett.* **115**, 028301 (2015).
- [9] A. Cavagna, D. Conti, C. Creato, L. Del Castello, I. Giardinina, T. S. Grigera, S. Melillo, L. Parisi, and M. Viale, *Nature Physics* **13**, 914 (2017).
- [10] A. Sokolov, L. D. Rubio, J. F. Brady, and I. S. Aranson, *Nature communications* **9**, 1 (2018).
- [11] A. G. Cherstvy, O. Nagel, C. Beta, and R. Metzler, *Physical Chemistry Chemical Physics* **20**, 23034 (2018).
- [12] A. Lagarde, N. Dagès, T. Nemoto, V. Démery, D. Bartolo, and T. Gibaud, *Soft Matter* **16**, 7503 (2020).
- [13] P. T. Underhill, J. P. Hernandez-Ortiz, and M. D. Graham, *Phys. Rev. Lett.* **100**, 248101 (2008).
- [14] Z. Liao, M. Han, M. Fruchart, V. Vitelli, and S. Vaikunathan, *The Journal of chemical physics* **151**, 194108 (2019).
- [15] D. Breoni, M. Schmiedeberg, and H. Löwen, *Phys. Rev. E* **102**, 062604 (2020).
- [16] Y. Hatwalne, S. Ramaswamy, M. Rao, and R. A. Simha, *Phys. Rev. Lett.* **92**, 118101 (2004).
- [17] S. Belan and M. Kardar, *The Journal of Chemical Physics* **150**, 064907 (2019).
- [18] A. R. Dulaney and J. F. Brady, *Phys. Rev. E* **101**, 052609 (2020).
- [19] P. Le Doussal, S. N. Majumdar, and G. Schehr, *EPL (Europhysics Letters)* **130**, 40002 (2020).
- [20] S. C. Takatori, R. De Dier, J. Vermant, and J. F. Brady, *Nature communications* **7**, 1 (2016).
- [21] P. Dolai, A. Das, A. Kundu, C. Dasgupta, A. Dhar, and K. V. Kumar, *Soft Matter* **16**, 7077 (2020).
- [22] F. Peruani, J. Starruß, V. Jakovljevic, L. Søggaard-Andersen, A. Deutsch, and M. Bär,

- Phys. Rev. Lett. **108**, 098102 (2012).
- [23] A. B. Slowman, M. R. Evans, and R. A. Blythe, Phys. Rev. Lett. **116**, 218101 (2016).
- [24] M. Kourbane-Houssene, C. Erignoux, T. Bodineau, and J. Tailleur, Phys. Rev. Lett. **120**, 268003 (2018).
- [25] S. Dal Cengio, D. Levis, and I. Pagonabarraga, Phys. Rev. Lett. **123**, 238003 (2019).
- [26] M. J. Metson, M. R. Evans, and R. A. Blythe, Journal of Statistical Mechanics: Theory and Experiment **2020**, 103207 (2020).
- [27] X.-q. Shi, G. Fausti, H. Chaté, C. Nardini, and A. Solon, Phys. Rev. Lett. **125**, 168001 (2020).
- [28] T. Agranov, S. Ro, Y. Kafri, and V. Lecomte, Journal of Statistical Mechanics: Theory and Experiment **2021**, 083208 (2021).
- [29] O. Chepizhko and F. Peruani, Phys. Rev. Lett. **111**, 160604 (2013).
- [30] D. Levis and L. Berthier, Phys. Rev. E **89**, 062301 (2014).
- [31] A. Liluashvili, J. Ónody, and T. Voigtmann, Phys. Rev. E **96**, 062608 (2017).
- [32] T. Bertrand, Y. Zhao, O. Bénichou, J. Tailleur, and R. Voituriez, Phys. Rev. Lett. **120**, 198103 (2018).
- [33] S. Put, J. Berx, and C. Vanderzande, Journal of Statistical Mechanics: Theory and Experiment **2019**, 123205 (2019).
- [34] P. Singh and A. Kundu, Journal of Physics A: Mathematical and Theoretical **54**, 305001 (2021).
- [35] V. E. Debets, X. M. de Wit, and L. M. C. Janssen, Phys. Rev. Lett. **127**, 278002 (2021).
- [36] P. Rizkallah, A. Sarracino, O. Bénichou, and P. Illien, Phys. Rev. Lett. **128**, 038001 (2022).
- [37] O. Granek, Y. Kafri, and J. Tailleur, Physical Review Letters **129**, 038001 (2022).
- [38] C. Kurzthaler, C. Devailly, J. Arlt, T. Franosch, W. C. K. Poon, V. A. Martinez, and A. T. Brown, Phys. Rev. Lett. **121**, 078001 (2018).
- [39] E. Irani, Z. Mokhtari, and A. Zippelius, Phys. Rev. Lett. **128**, 144501 (2022).
- [40] T. Bodineau and B. Derrida, Physical review letters **92**, 180601 (2004).
- [41] L. Bertini, A. De Sole, D. Gabrielli, G. Jona-Lasinio, and C. Landim, Physical Review Letters **87**, 040601 (2001).
- [42] C. Kipnis and C. Landim, *Scaling limits of interacting particle systems*, Vol. 320 (Springer Science & Business Media, 1998).
- [43] H. Spohn, *Large scale dynamics of interacting particles* (Springer Science & Business Media, 2012).
- [44] C. Arita, P. L. Krapivsky, and K. Mallick, Phys. Rev. E **90**, 052108 (2014).
- [45] J. M. Carlson, E. R. Grannan, and G. H. Swindle, Phys. Rev. E **47**, 93 (1993).
- [46] K. Malakar, V. Jemseena, A. Kundu, K. V. Kumar, S. Sabhapandit, S. N. Majumdar, S. Redner, and A. Dhar, Journal of Statistical Mechanics: Theory and Experiment **2018**, 043215 (2018).
- [47] A. Slowman, M. Evans, and R. Blythe, Journal of Physics A: Mathematical and Theoretical **50**, 375601 (2017).
- [48] A. Das, A. Dhar, and A. Kundu, Journal of Physics A: Mathematical and Theoretical **53**, 345003 (2020).
- [49] Y. Fily and M. C. Marchetti, Phys. Rev. Lett. **108**, 235702 (2012).
- [50] G. S. Redner, M. F. Hagan, and A. Baskaran, Phys. Rev. Lett. **110**, 055701 (2013).
- [51] M. J. Schnitzer, Phys. Rev. E **48**, 2553 (1993).
- [52] G. H. Weiss, *Physica A: Statistical Mechanics and its Applications* **3**, 1 (1976).
- [53] Supplemental Material available at....
- [54] In the limit $\psi \rightarrow 0$ ($\rho \ll \gamma$), the dynamics in fact reduces to the well known simple symmetric exclusion process (SSEP), in which case $P(g) \sim (1 - \rho)^g$ and the corresponding typical gap size is given by $g_* = -1/\ln(1 - \rho) \simeq 1/\rho$, which is the average interparticle spacing..
- [55] S. Chakraborti, T. Chakraborty, A. Das, R. Dandekar, and P. Pradhan, Phys. Rev. E **103**, 042133 (2021).
- [56] R. Soto and R. Golestanian, Phys. Rev. E **89**, 012706 (2014).
- [57] S. Katz, J. L. Lebowitz, and H. Spohn, Journal of statistical physics **34**, 497 (1984).
- [58] R. Mandal, P. J. Bhuyan, P. Chaudhuri, C. Dasgupta, and M. Rao, Nature communications **11**, 2581 (2020).
- [59] G. Szamel, Physical Review E **90**, 012111 (2014).
- [60] C. Maggi, U. M. B. Marconi, N. Gnan, and R. Di Leonardo, Scientific reports **5**, 1 (2015).
- [61] R. Dandekar, S. Chakraborti, and R. Rajesh, Phys. Rev. E **102**, 062111 (2020).